

Two coordinatively linked supramolecular assemblies constructed from highly electron deficient porphyrins

Kathryn E. Splan¹, Charlotte L. Stern, Joseph T. Hupp^{*}

Department of Chemistry, Northwestern University, 2145 Sheridan Road, Evanston, IL 60208, USA

Received 21 May 2004; accepted 26 June 2004

Available online 1 October 2004

Dedicated to Professor Tobin J. Marks on the occasion of his 60th birthday

Abstract

The synthesis of a pair of electron-deficient porphyrin building blocks and their resulting coordinatively linked supramolecular assemblies are described. The perfluorophenyl substituted porphyrins feature pendant pyridines which, upon reaction with $\text{Re}(\text{CO})_5\text{Cl}$ assemble into discrete dimers and tetramers, as dictated by the geometry of the porphyrin monomer. The resulting supramolecular complexes as well as their constituent porphyrins display several interesting and potentially useful properties owing to the electron-withdrawing nature of the perfluorophenyl functionalities. Structural, spectroscopic, and electrochemical data indicate that the electron-deficient porphyrins remain planar, allowing for modulation of spectral and redox properties, as well as for enhancement of the affinity of the porphyrins for Lewis-basic ligands.

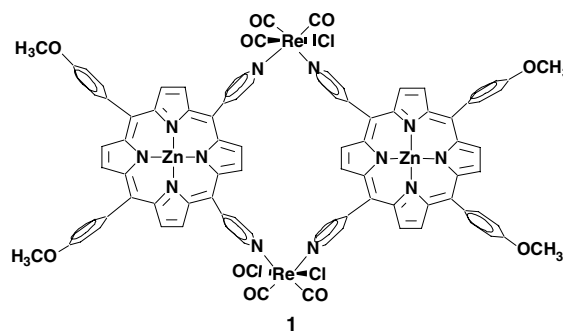
© 2004 Elsevier B.V. All rights reserved.

Keywords: Porphyrins; Supramolecular complexes; Electrochemistry

1. Introduction

Multiporphyrin arrays have proved to be an enormous field of recent interest [1]. First and foremost, porphyrins' close resemblance to natural light-harvesting chromophores have pushed them to the forefront of biomimetic studies of Nature's photosynthetic system and artificial photosynthesis [2–5]. Since then, numerous applications involving multiporphyrin systems have emerged. Porphyrins have been used in metallacyclic architectures as structural building blocks [6,7], sensor arrays [8], and molecular electronics components [9]. Recent efforts in our group have focused on the assembly of porphyrin compounds based on rhenium–pyridine coordination for a variety of applications [10–15]. For example, a series

of dyads – variants of compound **1** – have been studied as donor–acceptor complexes for energy transfer studies [11]. Molecular square **2** can function as a component of an artificial enzyme for epoxidation catalysis [12] and forms thin films capable of size selective permeant transport [13]. Closely related assemblies have been shown to form free-standing polymeric membranes [14], while still others are being used for photovoltaic applications [15].

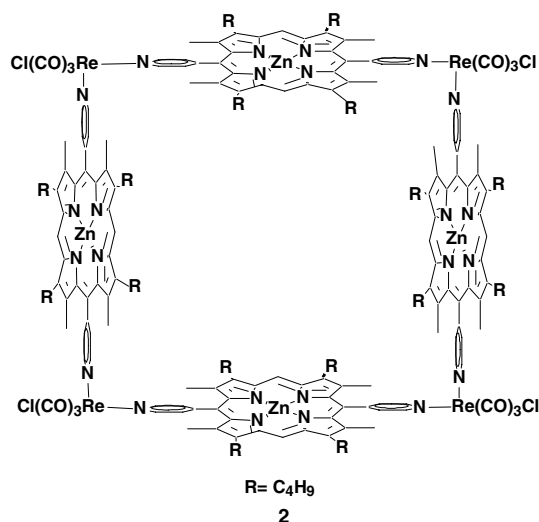


^{*} Corresponding author. Tel.: +847 491 3504; fax: +847 467 1425.

E-mail addresses: k-splan@chem.nwu.edu (K.E. Splan), j-hupp@northwestern.edu (J.T. Hupp).

¹ Tel.: +847 467 4931.

Recent advances in synthetic chemistry allow for functionalization of porphyrin compounds in a remarkably broad variety of ways [16]. Porphyrin building blocks can be designed to assemble spontaneously in predictable, well defined, and organized ways, and can be further functionalized to exhibit particular properties. Specifically, highly electron-deficient porphyrins containing halogen functionalities have been the subject of much research [17–21]. The electronegativity of the substituents engenders unique structural and electronic changes that can alter function. For example, polyhaloporphyrins can display enhanced catalytic activity for oxidation reactions [19], while fluorine substitution, in particular, has also been found to play a modulating role in energy and electron transfer rates through multiporphyrin arrays [22,23]. Herein we describe a pair of electron-deficient porphyrin building blocks (Scheme 1, **3** and **4**) and two resulting supramolecular assemblies (**5** and **6**). The compounds display many of the interesting and advantageous characteristics of other halogen-functionalized porphyrins, and their implications are discussed in the context of applications.



2. Experimental section

2.1. Synthesis and characterization

The synthesis of porphyrin compounds **3–6** is outlined in Scheme 1 and is detailed below. The synthesis of **3a** and **4a** is similar to a previous report [24]. All reagents were used as received unless otherwise specified.

2.1.1. 5,10-bis(pentafluorophenyl)-15,20-di(4-pyridyl)porphyrin (**3a**, *cis* isomer) and 5,15-bis(pentafluorophenyl)-10,20-di(4-pyridyl)porphyrin (**4a**, *trans* isomer)

Pentafluorobenzaldehyde (4.909 g, 0.025 mol), freshly distilled 4-pyridinecarboxaldehyde (2.678 g, 0.025 mol), and pyrrole (3.357, 0.050 mol) were added to 150 mL of

propionic acid. The mixture was deoxygenated by bubbling for 10 min with N₂ and then refluxed for 2 h. The solution volume was reduced by rotary evaporation and methanol was added to precipitate the products, yielding a mixture of six porphyrin isomers. The mixture was loaded onto a silica column and the desired products were eluted with 30:1 CHCl₃:EtOH. The *trans* and *cis* isomers eluted as the third and fourth band, respectively.

2.1.1.1. Characterization of 3a (cis isomer). Column chromatography yielded only trace amounts (<1%); therefore the product was collected and combined from several reactions. ¹H NMR (CDCl₃, 400 MHz): 12.10 (s, 2H), 9.08 (d, 4H, *J* = 5.9 Hz), 8.86 (dd, 8H, *J* = 7.3 Hz), 8.17 (d, 4H, *J* = 5.9 Hz) ppm. *Anal.* Calc. for C₄₂H₁₈N₆F₁₀: C, 63.31; H, 2.28; N, 10.55. Found: C, 63.31; H, 2.28; N, 10.37%. HRMS (FAB): 797.1511 (MH⁺, *m/z* calculated), 797.1516 (*m/z* observed). UV–Vis (CH₂Cl₂): 414, 509, 540, 584, 647 nm. Fluorescence (THF): 648, 710 nm.

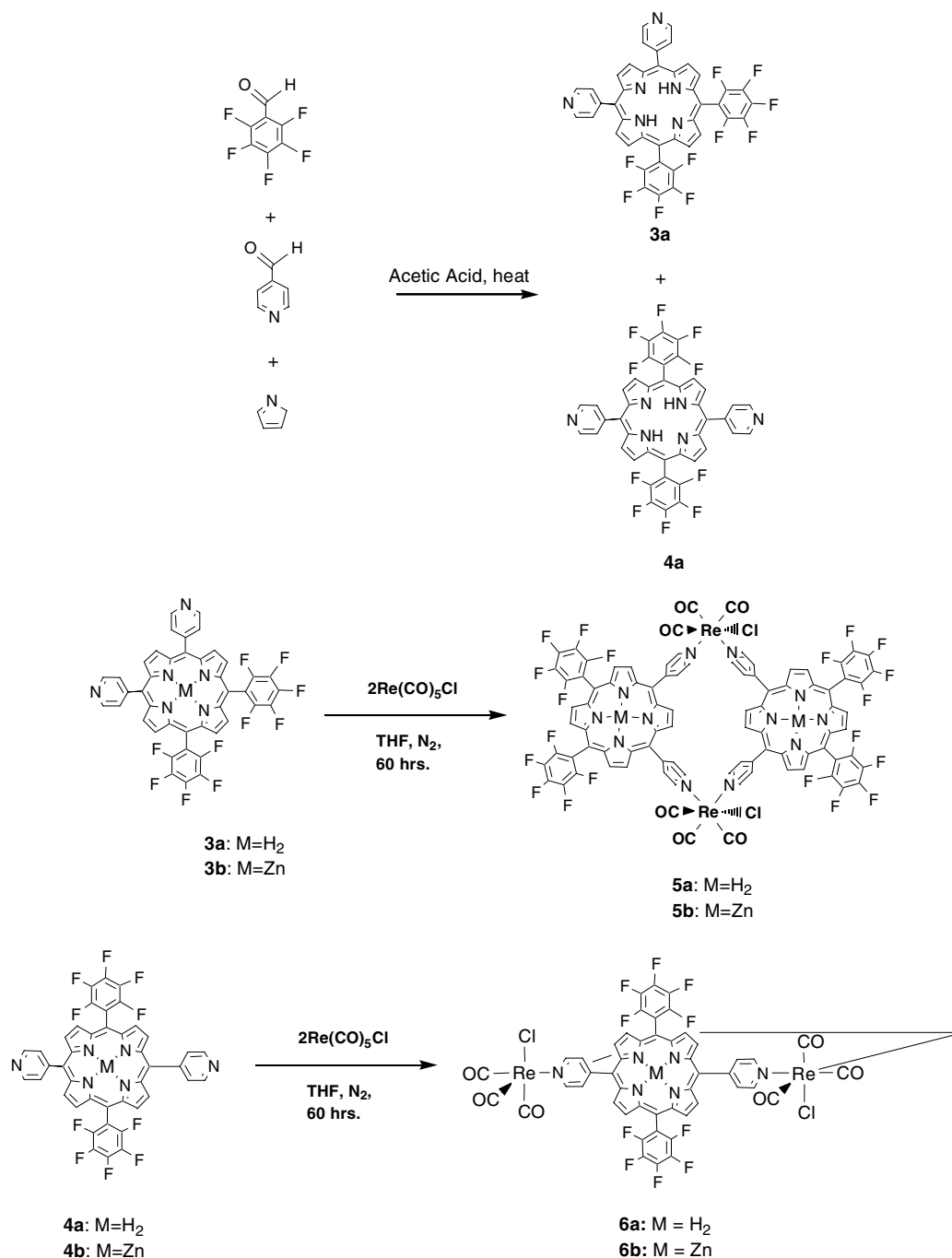
2.1.1.2. Characterization of 4a (trans isomer). Yield: 2%. ¹H NMR (CDCl₃, 400 MHz): 12.04 (s, 2H), 9.07 (d, 4H, *J* = 5.9 Hz), 8.87 (dd, 8H, *J* = 5.2 Hz), 8.17 (d, 4H, *J* = 5.9 Hz) ppm. *Anal.* Calc. for C₄₂H₁₈N₆F₁₀: C, 63.31; H, 2.28; N, 10.55. Found: C, 63.05; H, 2.56; N, 10.46%. UV–Vis (CH₂Cl₂): 414, 510, 540, 586, 646 nm. Fluorescence (THF): 649, 712 nm. LRMS (MALDI-TOF): 797.2 (MH⁺, *m/z* calculated), 797.9 (*m/z* observed).

2.1.2. [5,10-bis(pentafluorophenyl)-15,20-di(4-pyridyl)porphyrinato]zinc(II) (**3b**)

Zinc acetate (31.8 mg, 0.173 mmol) was dissolved in MeOH (5 mL) and added to **3a** (46.5 mg, 0.0584 mmol) in CHCl₃ (30 mL). The reaction stirred overnight in the dark. The solvent was removed under reduced pressure and the product recrystallized from THF/hexanes. Upon filtration, the purple solid was washed with 1:1 H₂O:MeOH (41.6 mg, 83% yield). ¹H NMR (CDCl₃/1 drop of py-*d*₅): 8.88 (d, 4H), 8.84 (d, 2H), 8.78 (m, 6H), 8.05 (d, 4H) ppm. LRMS (MALDI-TOF): 859.1 (MH⁺, *m/z* calculated), 859.2 (*m/z* observed). UV–Vis (CH₂Cl₂): 425, 556, 599 nm. Fluorescence (THF): 603, 656 nm.

2.1.3. [5,15-bis(pentafluorophenyl)-10,20-di(4-pyridyl)porphyrinato]zinc(II) (**4b**)

The synthesis is as described above for **3b**. Yield: 91%. ¹H NMR (Acetone-*d*₆/pyridine-*d*₅, 400 MHz): 9.21 (d, 4H, *J* = 5.1 Hz), 9.01 (d, 4H, *J* = 5.9 Hz), 8.98 (d, 4H, *J* = 5.1 Hz), 8.23 (d, 4H, *J* = 5.9 Hz) ppm. *Anal.* Calc. for C₄₂H₁₆N₆F₁₀ · H₂O: C, 57.53; H, 1.80; N, 9.59. Found: C, 57.36; H, 1.80; N, 9.52%. LRMS (MALDI-TOF): 859.1 (MH⁺, *m/z* calculated), 859.6 (*m/z* observed). UV–Vis (THF): 420, 552, 588 nm. Fluorescence (THF): 604, 658 nm.



Scheme 1. Synthesis of porphyrin compounds 3–6.

2.1.4. *Re(CO)₃(μ-(5,10-bis(pentafluorophenyl)-15,20-di(4-pyridyl)porphyrin)Cl)₂ (5a)*

3a (30.6 mg, 0.0384 mmol) and $\text{Re(CO)}_5\text{Cl}$ (14.3 mg, 0.0395 mmol) were refluxed under N_2 in distilled THF (25 mL) for 48 h. Upon cooling to room temperature, hexanes were added to precipitate the product, which was obtained as a purple solid (34.3 mg, 81%). ^1H NMR (CDCl_3 , 400 MHz): 10.00 (br, 4H), 9.53 (br, 4H), 9.18 (d, 4H, $J = 4.4$ Hz), 9.05 (d, 4H, $J = 4.4$ Hz), 8.99 (s, 4H), 8.94 (s, 4H), 8.56 (br, 4H), 8.44 (br, 4H)

ppm. LRMS (FAB): 2204.6 (MH^+ m/z , calculated), 2204.0 (m/z , observed). UV–Vis (THF): 422, 512, 588, 544, 644. Fluorescence (THF): 660, 718 nm.

2.1.5. [*Re(CO)₃(μ-(5,10-bis(pentafluorophenyl)-15,20-di(4-pyridyl)porphyrinato)zinc(II)Cl)₂ (5b)*]

Zinc acetate (10.6 mg, 0.0578 mmol) was dissolved in MeOH (5 mL) and added to **5a** (26.4 mg, 0.0120 mmol) in CHCl_3 (25 mL). The reaction mixture was stirred overnight in the dark. The product precipitated upon

the addition of MeOH to yield 12.7 mg. ^1H NMR (Acetone- d_6 , 400 MHz): 9.78 (d, 4H, $J = 5.1$ Hz), 9.56 (d, 4H, $J = 5.9$ Hz), 9.36 (s, 4H), 9.25 (d, 4H, $J = 4.4$ Hz), 9.21 (d, 4H, $J = 5.1$ Hz), 9.16 (s, 4H), 8.65 (d, 4H, $J = 5.1$ Hz), 8.58 (d, 4H, $J = 5.1$ Hz) ppm. UV–Vis (acetone): 422, 554, 596. Fluorescence (THF): 615, 662 nm.

2.1.6. $[\text{Re}(\text{CO})_3(\mu-(5,15\text{-bis}(\text{pentafluorophenyl})\text{-}10,20\text{-di}(4\text{-pyridyl))\text{porphyrin}))\text{Cl}]_4$ (**6a**)

4a (56.6 mg, 0.0711 mmol) and $\text{Re}(\text{CO})_5\text{Cl}$ (26.1 mg, 0.0721 mmol) were refluxed under N_2 in distilled THF for 48 h. Upon cooling to room temperature, hexanes were added to precipitate the product, which was obtained as a purple solid (66.5 mg, 85%). ^1H NMR (Acetone- d_6 , 400 MHz): 9.60 (d, 16H, $J = 6.6$ Hz), 9.24 (br, 32H), 8.70 (d, 16H, $J = 6.6$ Hz) ppm. *Anal. Calc.* for $\text{C}_{180}\text{H}_{72}\text{N}_{24}\text{F}_{40}\text{O}_{12}\text{Re}_4\text{Cl}_4 \cdot 4\text{H}_2\text{O}$: C, 47.45; H, 1.95; N, 7.38. Found: C, 47.43; H, 2.02; N, 7.18%. LRMS (FAB): 4410.2 (MH^+ m/z , calculated), 4410.8 (m/z , observed). FT-IR (THF): $\nu_{\text{CO}} = 2023, 1921, 1886 \text{ cm}^{-1}$. UV–Vis (CH_2Cl_2): 418, 510, 586 nm. Fluorescence (THF): 664, 714 nm.

2.1.7. $[\text{Re}(\text{CO})_3(\mu-([5,15\text{-bis}(\text{pentafluorophenyl})\text{-}10,20\text{-di}(4\text{-pyridyl))\text{porphyrinato}]\text{zinc}(\text{II}))\text{Cl}]_4$ (**6b**)

4b (56.4 mg, 0.0656 mmol) and $\text{Re}(\text{CO})_5\text{Cl}$ (25.2 mg, 0.0697 mmol) were treated as above for **6a**. Yield (68.9 mg, 90%). ^1H NMR (Acetone- d_6 , 400 MHz): 9.56 (d, 16H, $J = 6.6$ Hz), 9.17 (dd, 32H, $J = 4.4$), 8.64 (d, 16H, $J = 5.9$ Hz) ppm. *Anal. Calc.* for $\text{C}_{180}\text{H}_{64}\text{N}_{24}\text{F}_{40}\text{O}_{12}\text{Re}_4\text{Cl}_4\text{Zn}_4 \cdot 8\text{H}_2\text{O}$: C, 44.98; H, 1.68; N, 6.99. Found: C, 44.23; H, 1.39; N, 6.92%. LRMS (FAB): 4663.7 (MH^+ m/z , calculated), 4663.7 (m/z , observed). FT-IR (KBr): $\nu_{\text{CO}} = 2025, 1927, 1887 \text{ cm}^{-1}$. UV–Vis (acetone) λ_{max} (ϵ) [$\text{nm} (\text{cm}^{-1} \text{M}^{-1})$] 422 (1,000,000), 552 (79,000). Fluorescence (CH_2Cl_2): 614, 650 nm.

2.2. Instrumentation and methods

Elemental analyses were performed by Atlantic Microlabs, Inc. (Norcross, GA). Mass spectrometry data were obtained from the University of Illinois, Urbana-Champaign Mass Spectrometry Center. ^1H NMR spectra were collected on a Mercury 400 MHz spectrometer. Electronic absorption spectra were recorded on a Hewlett Packard HP8452A diode array UV–Vis spectrophotometer or a Varian Cary 5000 UV–Vis–NIR spectrophotometer. Steady-state fluorescence measurements were performed on a Jobin Yvon-SPEX Fluorolog-3 spectrofluorimeter. Electrochemical data were obtained using a CH Instruments potentiostat and plotted using CHI version 1202 software. Unless otherwise stated all measurements were conducted in dimethyl formamide with 0.1 M tetrabutylammonium hexafluorophosphate (TBAPF_6) as supporting electrolyte using a glassy carbon working electrode, platinum counter electrode, and Ag/AgCl

pseudo-reference electrode. All potentials were measured versus ferrocene and then adjusted to SCE based on $\text{Ferr}^{+/0} = 0.31$ versus SCE in acetonitrile [25].

2.3. X-ray crystallography

X-ray quality crystals of **4a** were grown from a CHCl_3 solution inside a capped NMR tube. Crystal data are presented in Table 1. Data were collected using a Bruker SMART detector and processed using SAINT-NT from Bruker. The structure was solved by direct methods and expanded using Fourier techniques. The non-hydrogen atoms were refined anisotropically. The central hydrogens were refined isotropically, and the remaining hydrogen atoms were included in idealized positions. Neutral atom scattering factors [26], anomalous dispersion effect values [27], and mass attenuation coefficients [27] were taken from literature values. All calculations were performed using the Bruker SHELXTL crystallographic software package [28].

2.4. Binding constant (K_b) determination

K_b values for pyridyl ligands binding to porphyrin squares **2** and **6b** were determined by electronic absorp-

Table 1
Crystallographic data for **4a**

Chemical formula	$\text{C}_{42}\text{F}_{10}\text{N}_6\text{H}_{18} \cdot 2(\text{CHCl}_3)$
Formula weight (g/mol)	1035.38
Crystal color, habit	red, plate
Lattice parameters	
a (Å)	6.7009(13)
b (Å)	10.305(2)
c (Å)	15.330(3)
α (°)	86.739(3)
β (°)	85.306(3)
γ (°)	77.309(3)
Temperature (K)	153 (2)
Wavelength (Å)	0.71073
Space group	$P\bar{1}$
Crystal dimensions (mm)	$0.38 \times 0.16 \times 0.05$
Crystal system	triclinic
Volume (Å ³)	1028.4(3)
Z value	2
D_{calc} (g/cm ³)	1.672
Radiation MoK α λ (Å)	0.7107
Graphite monochromated	
Absorption coefficient (mm ⁻¹)	0.507
Maximum and minimum transmission factors	0.9778 and 0.8844
Absorption correction	integration
$F(000)$	518
2θ Range	$1.33\text{--}28.28^\circ$
Reflections collected	9474
Unique reflections	4760
Refinement method	full-matrix least-squares on F^2
Final R indices	0.0444 (R_1), 0.1099 (wR_2)
R indices (all data)	0.0644 (R_1), 0.1290 (wR_2)
Goodness-of-fit indicator	1.54

tion titration. For example, 10 μL aliquots of a 3.1 mM solution of 4-phenylpyridine in CH_2Cl_2 were added to 2 mL of a 2.0 μM solution of **6b** in CHCl_3 and the absorbance at 422 nm was recorded after each addition. The data were fit to the following equation to obtain a value for K_b :

$$I_{\text{obs}} = \frac{(K_b^*[\text{guest}]^* \Delta I)}{(I + (K_b^*[\text{guest}]^*))} + I_o, \quad (1)$$

where I_{obs} is the absorbance observed after each aliquot addition, ΔI is the overall change in absorbance, and I_o is the initial absorbance. Eq. (1) assumes that for hosts capable of binding multiple guests, allosteric effects can be neglected. In applying the equation, account was taken of the decrease in concentration of the guest by guest:host association. For experiments in which CH_2Cl_2 was used as the solvent, the concentration of **6b** was estimated from the extinction coefficient measured in acetone, due to the low solubility of **6b** in CH_2Cl_2 .

3. Results and discussion

3.1. Synthesis and characterization

Free base porphyrins **3** and **4** were prepared via Adler–Longo conditions [29]. It should be noted that the compounds are briefly described in an earlier report by Aviezer and coworkers where they are used as synthetic intermediates [24]. Under these conditions, isomeric compounds in which the pyridyl groups are either *cis* (in the 5,10-positions) or *trans* (in the 5,15-positions) to each other are formed and can be isolated via careful column chromatography. Fluorinated porphyrin dimers **5** and tetramers **6** were synthesized as previously reported for related compounds **1** [11] and **2** [10]. Briefly, stoichiometric amounts of either *cis* or *trans* dipyrindyl porphyrins and $\text{Re}(\text{CO})_5\text{Cl}$ were refluxed for two days in THF to yield porphyrin dimers and squares, respectively. The presence of electron withdrawing fluorine groups on the monomers appeared not to greatly lower the Lewis-basicity of the pyridyl groups, as longer reaction times were not needed for the synthesis of **5** and **6** relative to **1** and **2**. Note also that several geometrical isomers are formed in the synthesis of **5** and **6** with respect to the chloro-ligand orientation; no attempts were made to separate these isomers.

3.2. X-ray crystallography studies

Although the isomers have the same mass, elemental composition, and photophysical properties, the identity of the compounds can usually be determined by characteristic NMR spectra [30]. However, **3** and **4** give extremely similar NMR spectra (not shown) leaving the

structural identity of the isolated isomers ambiguous. (Cleaner NMR-based assignments were reported, however, in [24] based on higher resolution measurements.) Fortunately, crystals of an isolated porphyrin compound, with mass spectral data corresponding to an isomer, were suitable for X-ray diffraction studies, and the compound was revealed to be the *trans* isomer. The refined crystal structure of **4a** is presented in Fig. 1 and selected bond lengths and angles are reported in Table 2. The structure reveals only a slightly ruffled porphyrin macrocycle, with the largest deviations being only 0.19 Å from the plane of the porphyrin ring (as defined by the four central nitrogen atoms). The pyridyl and perfluorophenyl groups are oriented at 68.3° and 73.3°, respectively, with regard to the plane of the porphyrin. In short, the structure is quite similar to that of free-base tetraphenyl porphyrin [31], implying that the electron-withdrawing nature of the substituents has little, if any, geometric structural impact. In contrast, porphyrins bearing perfluorinated alkyl chains at the *meso* and *beta* positions are characterized by strongly distorted and ruffled macrocycle structures, owing to unusual hydrogen bonding interactions between fluorocarbon fluorine atoms and porphyrin NH protons [21,32]. However, in the case of **4a** and other perfluorophenyl porphyrin compounds, the fluorine atoms of the phenyl groups lie above and below the plane of the porphyrin, thereby precluding any intermolecular interactions that might lead to ruffling [18]. Upon structural assignment of the isomers, the order of elution was established to be **4a** followed by **3a**. Surprisingly, the *trans* isomer **4a** was obtained in higher yield than the *cis* isomer **3a**, in contrast to the commonly observed threefold preference for *cis* isomer formation under the given experimental conditions [30].

3.3. Electronic structure effects

Although the perfluorophenyl groups have little effect upon core porphyrin geometries, their presence results in interesting *electronic* structural effects, which are best described by the four-orbital model for porphyrin ground and excited states [33,34]. The porphyrin lowest unoccupied molecular orbital (LUMO) consists of two degenerate orbitals of e_g symmetry, while the two highest occupied molecular orbitals (HOMOs) are assigned to a_{1u} and a_{2u} symmetry and are typically close in energy. When ${}^1\text{E}(a_{1u}, e_g)$ and ${}^1\text{E}(a_{2u}, e_g)$ are degenerate the two transitions partially cancel, resulting in a very low intensity band for the Q(0,0) transition, but leaving the higher energy Q(1,0) transition unaffected. As the degeneracy of the HOMOs is lifted the Q(0,0) band gains intensity; therefore the ratio of Q(1,0) intensity to Q(0,0) intensity reflects the energy difference between the a_{1u} and a_{2u} orbitals. The Q-band region of the electronic absorption spectrum for compound **3b** is shown

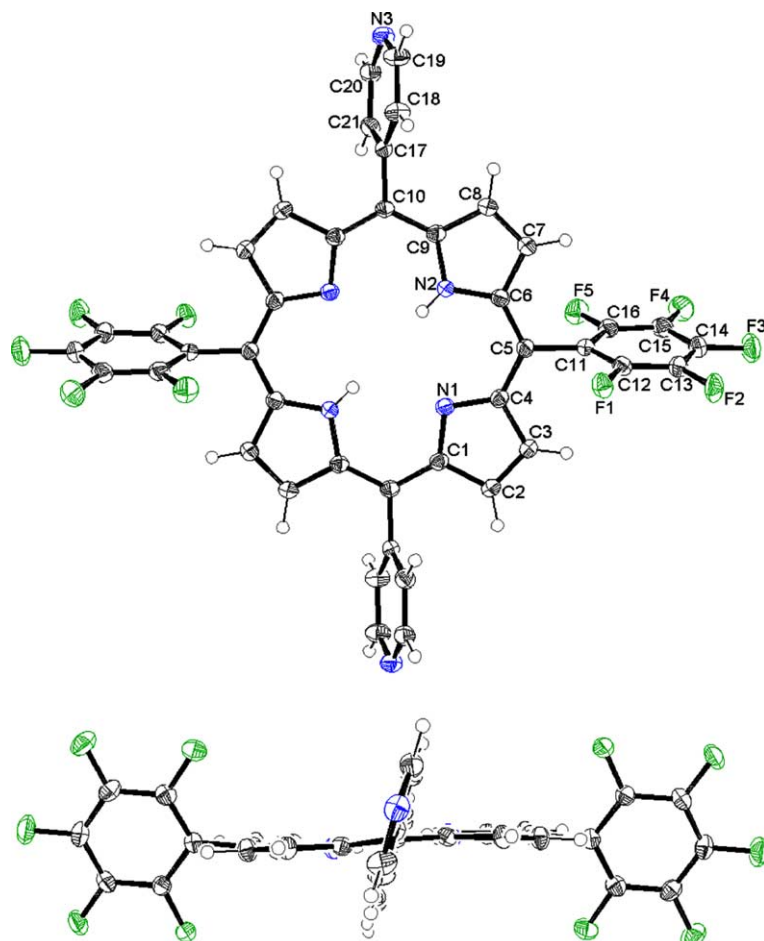


Fig. 1. ORTEP representation of **4a** showing both the front view (top) and side view (bottom) of the structure.

Table 2
Selected bond lengths and angles

Bond lengths (Å)		Bond angles (°)	
N(2)–H(1)	0.81 (3)	C(6)–N(2)–H(1)	126 (2)
N(2)–C(6)	1.371(3)	C(6)–N(2)–C(9)	109.8 (2)
C(6)–C(7)	1.434 (3)	N(2)–C(6)–C(5)	126.3 (2)
C(7)–C(8)	1.364 (3)	N(2)–C(6)–C(7)	107.0 (2)
C(5)–C(6)	1.397 (3)	C(8)–C(7)–C(6)	108.0 (2)
C(10)–C(17)	1.494 (3)	C(6)–C(5)–C(4)	126.6 (2)
C(5)–C(11)	1.494 (3)	C(5)–C(6)–C(7)	126.6 (2)

in Fig. 2, along with the spectrum for the zinc complex of 5,10,15,20-tetraphenyl porphyrin (ZnTPP). Relative to ZnTPP, the intensity ratio of the Q(1,0) and Q(0,0) transitions is large, with the Q(0,0) band appearing quite weak. This implies that the a_{2u} and a_{1u} orbitals are closer in energy in compound **3b** than in ZnTPP.

The different nodal pattern for the a_{1u} and a_{2u} orbitals revealed by electron density maps (Scheme 2, top) renders the orbital energies sensitive to substitution at the *meso* positions. Since the perfluorophenyl groups are strongly electron withdrawing, they should act to lower the orbital energy of a_{2u} relative to a_{1u} . Based on the

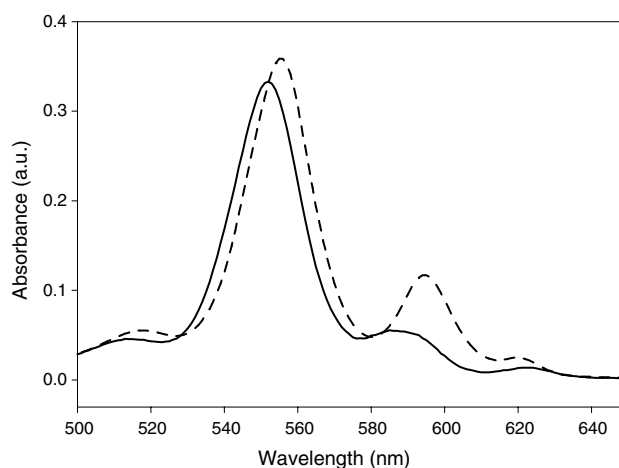
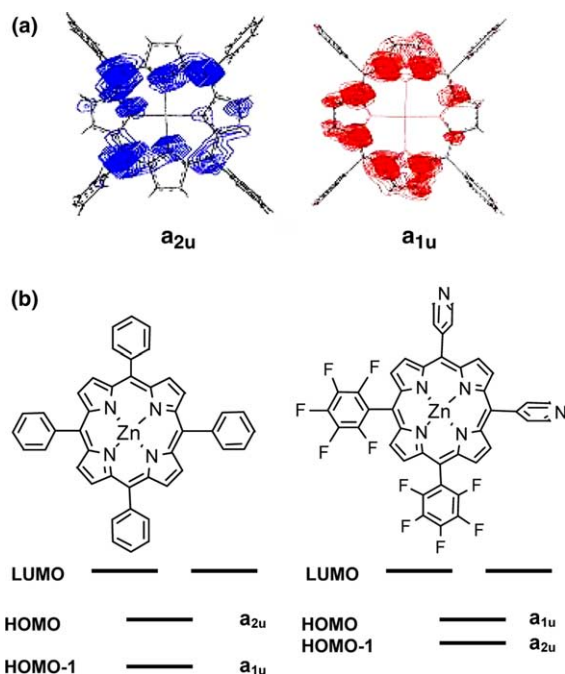


Fig. 2. Q-band region of the electronic absorption spectrum for compound **3b** (—) and ZnTPP (---) recorded in THF.

above discussion, the a_{1u} and a_{2u} orbitals are expected to be close in energy, and the relative orbital order is dependent on the porphyrin substituents. For example, electronic structure calculations show that the HOMO of the tetraphenylporphyrin zinc complex (ZnTPP) is



Scheme 2. (a) Electron density maps of molecular orbitals a_{1u} and a_{2u} . (b) Molecular orbital diagram describing the effects of perfluorophenyl substitution at the *meso* positions. The energy spacing between the HOMO and HOMO-1 is larger for ZnTPP than for **3a** and the orbital symmetry is reversed.

of a_{2u} symmetry [17], while the HOMO of **3b** is of a_{1u} symmetry [35]. Thus, as the phenyl groups of ZnTPP are replaced with perfluorophenyl groups, the a_{2u} orbital is lowered in energy such that the orbital order is reversed (Scheme 2, bottom). The ability to manipulate the orbital ordering, and thus, the electron density pattern, is an important tool in the rational design of molecular architectures that exploit electronic communication. Lindsey and co-workers have successfully modulated singlet energy transfer (EnT) within covalently linked porphyrin dyads via perfluorophenyl substitution at the *meso* positions [22]. Briefly, energy transfer was either: (a) kinetically inhibited by locating HOMO nodes (a_{1u} orbitals) at the *meso* carbon atoms used for covalent linkage of the donor and acceptor porphyrins, or (b) kinetically enhanced by locating nodes elsewhere (a_{2u} orbitals). Similar effects might be observed in asymmetric (i.e. partially metallated) analogues of **1** and **5** in which the difference in metallation creates a porphyrin/porphyrin excited-state energy difference.

3.4. Electrochemistry

The redox potentials of several of the fluorinated compounds were measured by cyclic voltammetry and compared to those of 4-methoxyphenyl-substituted *cis*-DPyP and **1**. The cyclic voltammograms of **3a** and *cis*-DPyP are shown in Fig. 3 and the electrochemical data

is summarized in Table 3. Consistent with previous reports [18,20], the electron withdrawing nature of the perfluorophenyl groups causes a positive shift in the oxidation and reduction potentials for both the porphyrin monomers and dimers, relative to the methoxyphenyl substituted compounds. While the reduction potentials are shifted positive by an average of 175 mV, the effect is more dramatic for the oxidation potentials; shifts of nearly 400 and 300 mV are observed for the porphyrin and the dimer, respectively. (We have assumed that the shifts in oxidation potential for these chemically irreversible processes reasonably approximate the thermodynamically significant shifts that would be obtained if the reactions were reversible.) Owing to the symmetry, and therefore, the nodal patterns of the a_{1u} and a_{2u} and e_g orbitals, it follows that the potentials for oxidation compounds should be more susceptible to modulation via electron withdrawing (or donating) functionalities than those for reduction.

While electron-withdrawing groups are capable of stabilizing the porphyrin HOMO (as reflected in the oxidation potential), the extent of the affect is dependent on the structural characteristics of the compound as well. Non-planar distortions of the porphyrin ring previously

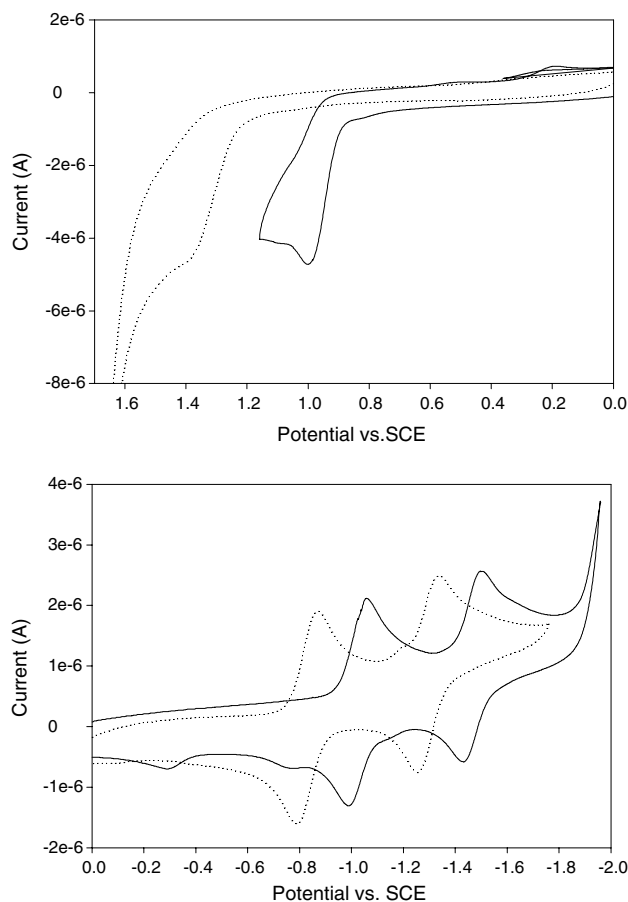


Fig. 3. Cyclic voltammograms in the oxidation (top) and reduction (bottom) regions for **3a** (···) and *cis*-DPyP (—).

Table 3
Electrochemistry data for selected compounds

Compound	$E_{\text{ox1}}(\text{V})^{\text{a}}$	$E_{\text{red1}}(\text{V})^{\text{a}}$	$E_{\text{red2}}(\text{V})^{\text{a}}$
cis-DPyP	0.94	-1.10	-1.54
3a	1.33	-0.91	-1.38
1	1.02	-1.01	n.a. ^b
5a	1.31	-0.85	n.a. ^b

^a V versus SCE. All data were taken in 0.1 M TBAPF₆ DMF electrolyte versus pseudo Ag/AgCl. Ferrocene was used as an internal standard to convert all values to SCE reference.

^b The second reduction potential for the porphyrin dimer compounds was ambiguous owing to the Re(I/O) couple at similar potentials and is not reported.

observed with bulky fluorinated substituents are known to raise the HOMO energy, partially counteracting the gains made by electron-withdrawing substitution [21,32]. For example, the oxidation potential of 2-bromo-H₂TPP is shifted 80 mV positive with respect to H₂TPP [36], while the addition of seven more bromine atoms further shifts the potential by only 220 mV [37]. The absence of planar distortions for **4a** allows for the substantial 400 mV shift in apparent oxidation potential upon addition of only two perfluorophenyl groups and reiterates the virtues of structural invariance when seeking to modulate the electronic properties via ligand substitution.

3.5. Binding studies of porphyrin dimers and squares

Molecular squares **2** and **6b** are capable of binding a wide variety of pyridine-based guests via Zn axial ligation. Upon exposure to excess 4-phenylpyridine in chloroform as solvent the Soret band of **6b** at 422 nm experiences an 8 nm red-shift, indicative of zinc ligation (Fig. 4). Only four, rather than eight, equivalents of guest are expected to bind because of the preference of Zn (II) for fivefold coordination. The binding constant for 4-phenylpyridine in **6b** was measured via an electronic absorption titration (Fig. 4, inset). The data were fit to Eq. (1) to yield a K_b value of $(1.35 \pm 0.09) \times 10^5 \text{ M}^{-1}$, nearly an order of magnitude higher than for **2** as host ($K_b = 1.5 \times 10^4 \text{ M}^{-1}$). The perfluorophenyl groups significantly increase the Lewis acidity of the zinc center, resulting in an increased affinity for Lewis basic pyridyl compounds. Also, the porphyrin-square/pyridyl-ligand interaction is highly dependent on solvent, as the binding constant for 4-phenylpyridine in **6b** is found to be over an order of magnitude smaller in acetone, a moderately basic solvent that can compete to some degree for the zinc binding site. Thus, in order to fully exploit the enhanced binding capabilities of complexes such as **6b** it is important that they be sufficiently soluble in non-coordinating solvents such as CH₂Cl₂ and CHCl₃.

Axial zinc binding is a helpful tool in the use of porphyrin compounds as functional assemblies, and the en-

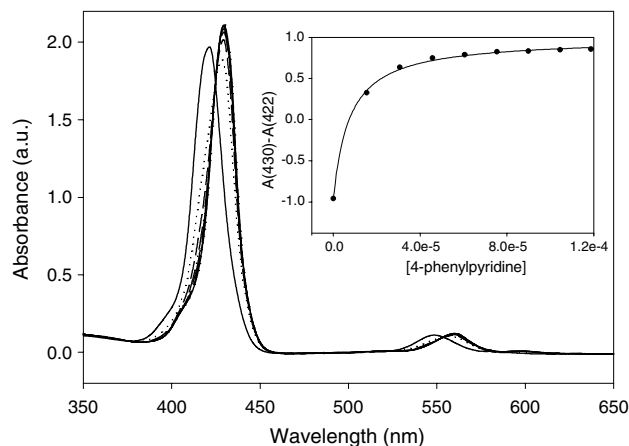
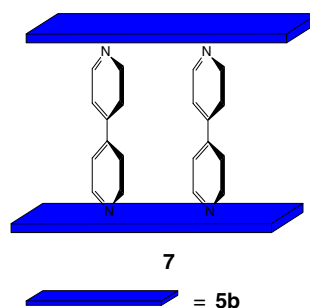


Fig. 4. Electronic absorption spectra of **6b** upon the addition of 4-phenylpyridine. Complete ligation by **6b** is indicated by an 8 nm red-shift in the Soret region. (Inset): Binding curve for the titration data. $K_b = (1.35 \pm 0.09) \times 10^5 \text{ M}^{-1}$.

hanced Lewis base affinity of **6b** is potentially useful. For example, encapsulation by **2** of di-pyridyl manganese porphyrin (MnDPyP), a known epoxidation catalyst, results in a 10–100-fold enhancement in catalyst lifetime (total turnover number), and further modification of the catalyst to increase its affinity for **2** results in even larger turn-over numbers [12]. Replacement of **2** with **6b** would be expected to further enhance catalyst performance.

Many construction schemes for multiporphyrin arrays rely on axial coordination [38–40], and such interactions can be enhanced to yield more robust structures by simple modification with electron-withdrawing functionalities. For example, upon treatment with one equivalent of a *trans* ditopic N-donor ligand, porphyrin dimers and oligomers similar to **1** and **5b** form discrete sandwich complexes in which the di-functional ligands form bridges between the porphyrin compounds [40,41]. The sandwich structure is thermodynamically favored over oligomeric structures or single point binding owing to a cooperative effect upon zinc center ligation. As a result, sandwich formation occurs on an all-or-nothing basis, as no intermediates are observed in the UV–Vis spectra [41].



Consistent with these reports, treatment of **5b** with stoichiometric amounts of 4,4'-bipyridine at micromolar concentrations results in spectral shifts indicative of zinc ligation. By analogy to the reports mentioned above for closely related compounds, association is believed to yield the sandwich structure **7**. Based on this assumption, the titration data can be analyzed using the fitting program SPECFIT/32TM to yield a formation constant (K_f) of $(2.8 \pm 1.2) \times 10^{18} \text{ M}^{-3}$, where K_f is defined as:

$$K_f = \frac{[\mathbf{5b}_2(\text{bipy})_2]}{[\mathbf{5b}]^2[\text{bipy}]^2} \quad (2)$$

This value is consistent with those reported for similar porphyrin dimers [41]. In contrast, addition of 4-phenylpyridine to micromolar amounts of **5b** is best modeled by 1:1 porphyrin:ligand complex formation, assuming that the porphyrin centers in each dimer behave independent of one another, as previously observed [41]. In this case a K_f value of $(1.8 \pm 0.2) \times 10^5 \text{ M}^{-1}$ is observed. It is difficult to compare the strengths of the two different interactions (sandwich formation versus single point binding) because the dimensions of K_f vary with different complexing species. A better point of comparison is to calculate the concentration, c_{50} , at which each complex is 50% dissociated. For complex **7**, c_{50} is calculated according to Eq. (3) [41]:

$$c_{50} = \frac{1}{(16K_f)^{1/3}} \quad (3)$$

For simple 1:1 complex formation with 4-phenylpyridine c_{50} is defined as $1/K_f$. Values of 2.8×10^{-7} and $5.6 \times 10^{-6} \text{ M}$ are observed for **7** and **5b**: 4-phenylpyridine, respectively. This order of magnitude difference reflects the cooperative nature of the formation of **7** versus single point binding. Note also, the enhanced basicity of 4-phenylpyridine ($\text{p}K_a = 5.55$) versus 4,4'-bipyridine ($\text{p}K_a = 4.82$) [42]. Comparisons with ligands having more precisely matched $\text{p}K_a$ values should yield somewhat larger differences in c_{50} values. Finally, a similar titration performed with 4,4'-bipyridine and **1**, again presumably leading to sandwich structure formation, yields K_f equal to $(3.1 \pm 0.5) \times 10^{16} \text{ M}^{-3}$ and c_{50} equal to $1.3 \times 10^{-6} \text{ M}$. The enhanced Lewis-acidity of **5b** relative to **1** clearly allows for the formation of a somewhat more robust supramolecular architecture.

4. Conclusions

In summary, *cis* and *trans* isomers of di-pyridyl porphyrin compounds featuring perfluorophenyl groups at two of the four *meso* positions have been prepared and reacted with $\text{Re}(\text{CO})_5\text{Cl}$ to form dimeric and tetrameric (square) porphyrin assemblies, respectively. The supramolecular assemblies as well as their constituent porphy-

rins display interesting and potentially usefully altered properties owing to the electron-withdrawing nature of the perfluorophenyl functionalities. Despite the presence of fluorine atoms, which increase the likelihood of intermolecular hydrogen bonding, the geometrical structures of the porphyrins remain relatively unperturbed. Therefore, it is possible for the electron-deficient substituents to alter the HOMO orbital energies significantly, as evidenced by substantial positive shifts in porphyrin oxidation potentials. The addition of perfluorophenyl groups enhances the affinity of porphyrin square **6b** for pyridine-based ligands owing to the increased Lewis acidity of the zinc center. This enhanced affinity can be exploited to form other supramolecular complexes such as **7**. Taken together, **3–7** illustrate in a straightforward way how modification of porphyrin compounds with electron-deficient substituents can impart or alter specific properties. Such modulation should prove useful in applications that require careful control over structural, electronic, and supramolecular properties.

Acknowledgements

We thank the Basic Energy Sciences Program, Office of Science, US Department of Energy (Grant No. DE-FG02-87ER13808) and the Dow Foundation (graduate fellowship to K.E.S.) for financial support of our research.

References

- [1] C.M. Drain, J.T. Hupp, K.S. Suslick, M.R. Wasielewski, *J. Porph. Phthalocyanines* 6 (2002) 243.
- [2] D. Gust, T.A. Moore, *Science* 244 (1989) 35.
- [3] H. Kurreck, M. Huber, *Angew. Chem. Int. Ed.* 34 (1995) 849.
- [4] D. Kuciauskas, P.A. Liddell, S. Lin, T.E. Johnson, S.J. Weghorn, J.S. Lindsey, A.L. Moore, T.A. Moore, D. Gust, *J. Am. Chem. Soc.* 121 (1999) 8604.
- [5] D. Gust, T.A. Moore, A.L. Moore, *Acc. Chem. Res.* 34 (2001) 40.
- [6] J. Fan, J.A. Whiteford, B. Olenyuk, M.D. Levin, P.J. Stang, E.B. Fleischer, *J. Am. Chem. Soc.* 121 (1999) 2741.
- [7] E. Iengo, B. Milani, E. Zangrando, S. Geremia, E. Alessio, *Angew. Chem. Int. Ed.* 39 (2000) 1096.
- [8] N.A. Rakow, K.S. Suslick, *Nature* 406 (2000) 710.
- [9] A.S. Lukas, P.J. Bushard, M.R. Wasielewski, *J. Am. Chem. Soc.* 123 (2001) 2440.
- [10] R.V. Slone, J.T. Hupp, *Inorg. Chem.* 36 (1997) 5422.
- [11] K.E. Splan, M.H. Keefe, A.M. Massari, K.A. Walters, J.T. Hupp, *Inorg. Chem.* 41 (2002) 619.
- [12] M.L. Merlau, W.J. Grande, S.T. Nguyen, J.T. Hupp, *J. Mol. Catal. A: Chem.* 156 (2000) 79.
- [13] S. Belanger, J.T. Hupp, *Angew. Chem. Int. Ed.* 38 (1999) 2222.
- [14] M.H. Keefe, J.L. O'Donnell, R.C. Bailey, S.T. Nguyen, J.T. Hupp, *Adv. Mater.* 15 (2003) 1936.
- [15] K.E. Splan, A.M. Massari, J.T. Hupp, *J. Phys. Chem. B* 108 (2004) 4111.
- [16] S. Shanmugathasan, C. Edwards, R.W. Boyle, *Tetrahedron* 56 (2000) 1025.

- [17] P.J. Spellane, M. Gouterman, A. Antipas, S. Kim, Y.C. Liu, *Inorg. Chem.* 19 (1980) 386.
- [18] E.K. Woller, S.G. DiMagno, *J. Org. Chem.* 62 (1997) 1588.
- [19] D. Dolphin, T.G. Traylor, L.Y. Xie, *Acc. Chem. Res.* 30 (1997) 251.
- [20] K.T. Moore, J.T. Fletcher, M.J. Therien, *J. Am. Chem. Soc.* 121 (1999) 5196.
- [21] V.V. Smirnov, E.K. Woller, D. Tatman, S.G. DiMagno, *Inorg. Chem.* 40 (2000) 2614.
- [22] J.P. Strachan, S. Gentemann, J. Seth, W.A. Kalsbeck, J.S. Lindsey, D. Holten, D.F. Bocian, *J. Am. Chem. Soc.* 119 (1997) 11191.
- [23] A. Willert, S. Bachilo, U. Rempel, A. Shulga, E. Zenkevich, C.v. Borczyskoski, *J. Photochem. Photobiol. A: Chemistry* 126 (1999) 99.
- [24] D. Aviezer, S. Cotton, M. David, A. Segev, N. Khaselev, N. Gahili, Z. Gross, A. Yayon, *Cancer Res.* 60 (2000) 2973.
- [25] A.J. Bard, L.R. Faulkner, *Electrochemical Methods: Fundamentals and Applications*, second ed., John Wiley & Sons Inc., New York, 2001.
- [26] D.T. Cromer, J.T. Waber, *International Tables for X-ray Crystallography*, vol. IV, The Kynoch Press, Birmingham, England, 1974.
- [27] D.C. Creagh, J.H. Hubbell, *International Tables for Crystallography*, vol. C, Kluwer Academic Publishers, Boston, 1992.
- [28] *SMART Version 5.054 Data Collection and SAINT-Plus Version 6.02A Data Processing Software for the SMART System*; Bruker Analytical X-ray Instruments: Madison, WI, 2000.
- [29] A.D. Adler, F.R. Longo, J.D. Finarelli, J. Goldmacher, J. Assour, L. Korsakoff, *J. Org. Chem.* 32 (1967) 476.
- [30] G.G. Meng, B.R. James, K.A. Skov, *Can. J. Chem.* 72 (1994) 1894.
- [31] S.J. Silvers, A. Tulinsky, *J. Am. Chem. Soc.* 89 (1967) 3331.
- [32] S.G. DiMagno, R.A. Williams, *J. Org. Chem.* 59 (1994) 6943.
- [33] M. Gouterman, *J. Chem. Phys.* 30 (1959) 1139.
- [34] M. Gouterman, in: D. Dolphin (Ed.), *The Porphyrins*, vol. III, Academic Press, New York, 1979, p. 1.
- [35] M.H. Keefe, Ph.D. thesis, Department of Chemistry, Northwestern University, 2001.
- [36] A. Giraudeau, H.J. Callot, M. Gross, *Inorg. Chem.* 18 (1979) 201.
- [37] P. Bhyrappa, V. Krishnan, *Inorg. Chem.* 30 (1991).
- [38] R.A. Haycock, A. Yartsev, U. Michelsen, V. Sundstrom, C.A. Hunter, *Angew. Chem. Int. Ed.* 39 (2000) 3616.
- [39] K. Ogawa, Y. Kobuke, *Angew. Chem. Int. Ed.* 39 (2000) 4070.
- [40] E. Iengo, E. Zangrando, R. Minatel, E. Alessio, *J. Am. Chem. Soc.* 124 (2002) 1003.
- [41] P.N. Taylor, H.L. Anderson, *J. Am. Chem. Soc.* 121 (1999) 11538.
- [42] S. Belanger, M.H. Keefe, J.L. Welch, J.T. Hupp, *Coord. Chem. Rev.* 190–192 (1999) 29.